

光学学报

对准标记鲁棒性分析方法及仿真

周光迎^{1,3}, 齐月静^{1,3*}, 李亮², 姜森², 师江柳², 么铭怡^{1,3}

¹中国科学院微电子研究所, 北京 100029;

²北京超弦存储器研究院, 北京 100176;

³中国科学院大学, 北京 100049

摘要 针对复杂结构对准标记仿真需求, 联合严格耦合波法和分层近似法提出一种对准标记鲁棒性分析方法。利用该方法构建仿真模型:以晶圆质量和信噪比为评价函数, 研究了标记槽深、槽宽、膜层厚度和侧壁对称变形等参数变化对标记鲁棒性的影响;以对准误差为评价函数, 研究了侧壁非对称变形对标记鲁棒性的影响。并结合对准标记鲁棒性分析结果明晰了光刻机提升标记工艺适应性的策略。最后借助 VirtualLab 商业软件和实验平台, 验证了分析方法的有效性和准确性。所提方法和给出的工艺适应性策略, 对于对准标记设计优化和光刻机对准精度提升具有重要的理论意义和应用价值。

关键词 光刻; 对准标记; 严格耦合波法; 分层近似法; 鲁棒性; 工艺适应性

中图分类号 O436

文献标志码 A

DOI: 10.3778/AOS222161

1 引言

随着光刻工艺节点的不断减小, 新材料和新工艺不断被引入^[1-2], 这对实现光刻机对准功能的对准标记会产生不同程度的影响, 提升对准标记的鲁棒性对于实现高精度对准至关重要。基于实验方法验证对准标记的鲁棒性会消耗大量时间和成本, 工业界倾向用仿真实验的方法来提高研究效率和经济性^[3-6]。为此, 本文开展对准标记鲁棒性仿真模型构建方法及案例分析, 对于提升效率和经济性具有重要的理论意义和应用价值。

对准标记仿真的理论基础可分为标量衍射理论和矢量衍射理论^[7]。杜聚有等^[6,8-11]基于标量衍射理论分析了简单对准标记槽深、槽宽、膜层厚度及侧壁倾角对衍射效率的影响。对于小周期或结构复杂的对准标记, 矢量衍射理论有着更好的计算精度。Shin 等^[12]基于严格耦合波法研究了膜层厚度对对准信号强度的影响。Yun 等^[13]基于严格耦合波法研究了光刻材料参数和膜层厚度对对准信号的影响。Ahn 等^[14]基于时域有限差分法研究了含侧壁倾角的对准标记膜层厚度对信号强度的影响。严格耦合波法相较于时域有限差分法有着更快的计算速度^[15], 但采用该方法求解因工艺产生变形的复杂结构对准标记时, 需要结合分层近似法^[16]。

本文结合复杂结构对准标记仿真需求, 联合严格

耦合波法和分层近似法提出一种对准标记鲁棒性分析方法, 并构建了仿真模型。以晶圆质量(W_Q)和信噪比(R_{SN})为评价函数, 研究了槽深、槽宽、膜层厚度和侧壁对称变形等参数对标记鲁棒性的影响; 以对准误差为评价函数, 研究了侧壁非对称变形对标记鲁棒性的影响。并结合对准标记鲁棒性的分析结果明晰了光刻机提升标记工艺适应性的策略。最后借助 VirtualLab 商业软件验证了所建模型的正确性, 并在光刻机上制作标记进行了实验测试, 验证了所提方法的有效性。

2 基本原理

为适应光刻工艺需求, 对准标记周期不断缩小。对于侧壁未变形的标记, 因其具有标准面型, 可采用严格耦合波法建立其矢量衍射仿真模型。对于因工艺影响产生侧壁变形的对准标记, 因其不再具有标准面型, 很难直接构建其面型函数。为此, 联合严格耦合波法和分层近似法提出一种对准标记鲁棒性分析方法, 以满足对准标记鲁棒性研究的需求。具体思路是将有侧壁变形的对准标记划分为等厚的若干层, 当划分的层数足够多时, 每一层可近似为矩形结构, 以多个矩形结构组成的整体来代替原来具有复杂结构的对准标记。每一层中的矩形结构按矩形光栅的方法分析, 联立每一层的边界条件求解, 最终求解出复杂结构对准标记的衍射效率。

图 1 是对准标记分层处理示意图, 其中, p 为光栅

收稿日期: 2022-12-20; 修回日期: 2023-01-17; 录用日期: 2023-02-10; 网络首发日期: 2023-03-09

通信作者: *qiyuejing@ime.ac.cn

周期, d 为光栅刻槽的深度, σ 为入射光照射到光栅上的入射角度, 区域1为入射区, 中间区域为光栅区, 区域2为透射区。基于分层近似法将光栅区域分为 L 层, 入射界面下为第1层, 次之为第2层, 依次类推, 最后一层为第 L 层。

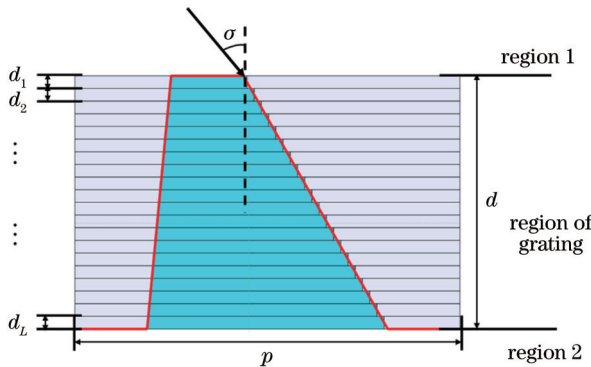


图1 对准标记分层处理示意图

Fig. 1 Schematic diagram for layered processing of alignment mark

对于光栅区域的每一层, 其介质为周期性分布, 即其介电常数为周期性函数, 介电常数傅里叶级数展开式为

$$\epsilon_l(x) = \sum_h \epsilon_{l,h} \exp\left(j \frac{2\pi}{p} h x\right), \quad (1)$$

式中, $\epsilon_{l,h}$ 为光栅区域内第 l 层介电常数的第 h 级傅里叶级数。

以TE偏振入射为例, 此时电场矢量平行于光栅刻槽方向, 根据Rayleigh展开式, 反射区域1和透射区域2的电场分布分别为

$$E_1 = \exp[-jk_0 n_0(x \sin \sigma + z \cos \sigma)] + \sum_m R_m \exp[-j(k_{xm}x - k_{1,zm}z)], \quad (2)$$

$$E_2 = \sum_m T_m \exp\{-j[k_{xm}x - k_{2,zm}(z - D_L)]\}, \quad (3)$$

式中: R_m 和 T_m 分别为第 m 级反射光和透射光的归一化电场振幅; 光栅刻槽的深度 $D_L = \sum_{p=1}^L d_p$; k_0 为入射光在真空中的波数; k_{xm} 为第 m 级 x 方向的波矢分量; $k_{1,zm}$ 和 $k_{2,zm}$ 分别表示反射区和透射区第 m 级 z 方向的波矢分量。

在第 l 层, 电场的 y 分量和磁场的 x 分量的空间谐波的傅里叶级数展开式为

$$E_{l,gy} = \sum_m S_{l,ym}(z) \exp(-jk_{xm}x), \quad (4)$$

$$H_{l,gx} = -j \left(\frac{\epsilon_0}{\mu_0} \right)^{1/2} \sum_m U_{l,xm}(z) \exp(-jk_{xm}x), \quad (5)$$

式中: $S_{l,ym}(z)$ 和 $U_{l,xm}(z)$ 分别表示第 l 层、第 m 级电场空间谐波和磁场空间谐波的归一化振幅, 其表达式为

$$S_{l,ym}(z) = \sum_{i=1}^n w_{l,m,i} \left\{ c_{l,i}^+ \exp[-k_0 q_{l,i}(z - D_l + d_i)] + c_{l,i}^- \exp[k_0 q_{l,i}(z - D_l)] \right\}, \quad (6)$$

$$U_{l,ym}(z) = \sum_{i=1}^n v_{l,m,i} \left\{ -c_{l,i}^+ \exp[-k_0 q_{l,i}(z - D_l + d_i)] + c_{l,i}^- \exp[k_0 q_{l,i}(z - D_l)] \right\}, \quad (7)$$

式中: $w_{l,m,i}$ 为矩阵 W_l 的元素; $q_{l,i}$ 是矩阵 A_l 的特征值的正平方根; W_l 为矩阵 A_l 的特征值向量^[16]; d_i 为第 l 层的厚度; 系数 $c_{l,i}^+$ 和 $c_{l,i}^-$ 需结合边界条件求得; $v_{l,m,i}$ 是矩阵 V_l 的元素, 该矩阵的表达式为

$$V_l = W_l Q_l. \quad (8)$$

在入射边界($z=0$)处, 有

$$\begin{bmatrix} \delta_{m0} \\ jn_1 \delta_{m0} \cos \sigma \end{bmatrix} + \begin{bmatrix} I \\ -jY_1 \end{bmatrix} [R] = \begin{bmatrix} W_1 & W_1 X_1 \\ V_1 & -V_1 X_1 \end{bmatrix} \begin{bmatrix} c_1^+ \\ c_1^- \end{bmatrix}. \quad (9)$$

在第 l 层和第 $l-1$ 层边界处($z=D_{l-1}$)处, 有

$$\begin{bmatrix} W_{l-1} X_{l-1} & W_{l-1} \\ V_{l-1} X_{l-1} & -V_{l-1} \end{bmatrix} \begin{bmatrix} c_{l-1}^+ \\ c_{l-1}^- \end{bmatrix} = \begin{bmatrix} W_l & W_l X_l \\ V_l & -V_l X_l \end{bmatrix} \begin{bmatrix} c_l^+ \\ c_l^- \end{bmatrix}. \quad (10)$$

在出射边界($z=D_L$)处, 有

$$\begin{bmatrix} W_L X_L & W_L \\ V_L X_L & -V_L \end{bmatrix} \begin{bmatrix} c_L^+ \\ c_L^- \end{bmatrix} = \begin{bmatrix} I \\ jY_2 \end{bmatrix} [T]. \quad (11)$$

联立式(9)~(11), 通过薄层光栅的系数之间存在的递推关系, 可得:

$$\begin{bmatrix} \delta_{m0} \\ jn_1 \delta_{m0} \cos \sigma \end{bmatrix} + \begin{bmatrix} I \\ -jY_1 \end{bmatrix} [R] = \prod_{l=1}^L \begin{bmatrix} W_l & W_l X_l \\ V_l & -V_l X_l \end{bmatrix} \begin{bmatrix} W_l X_l & W_l \\ V_l X_l & -V_l \end{bmatrix}^{-1} \begin{bmatrix} I \\ jY_2 \end{bmatrix} [T], \quad (12)$$

式中: n_1 为反射区域的折射率; δ_{m0} 为克罗内克尔函数。

联立各层、各区域的麦克斯韦方程和边界条件, 借助数学算法可以求解出 R 和 T 等数值, 从而求解出衍射效率。TM偏振情况下的衍射效率可参考上述计算过程得出, 其他偏振情况下的衍射效率可通过TE和TM偏振下衍射效率计算得到^[7]。

3 仿真分析

对准信号强度、对准信号信噪比和对准误差是影响测量精度的3个重要因素^[6,17]。在光刻机中, 一般用晶圆质量表示对准信号强度, 其与光栅衍射效率呈比例关系:

$$W_{Q,m} = \frac{\eta_m}{\eta_{1,fiducial}} \quad (13)$$

式中: $W_{Q,m}$ 表示第 m 级衍射光的晶圆质量; η_m 表示第 m 级衍射光的衍射效率; $\eta_{1,fiducial}$ 表示光刻机中 633 nm 波长下基准对准标记的1级衍射效率, 其数值约为 14.122%^[9,11]。

当对准系统以 $\pm m$ 级衍射光作为测量信号时, 不

同波长测量信号的信噪比^[7]可表示为

$$R_{SN,k} = \frac{2 \cdot \eta_m}{0.012 \cdot \eta_m + 0.003(2 \cdot \eta_{m-1} + \eta_0 + 2 \cdot \eta_{m+1})}, \quad k = \lambda_1, \lambda_2, \dots, \lambda_N. \quad (14)$$

当对准标记发生非对称变形时,测量波长的正负衍射光束之间会引入额外的相位信息,造成正负测量光束衍射效率不同,引入对准误差,且对准误差 Δx 与正负测量光束衍射效率之差成正比^[9],其表达式为

$$\Delta x \propto \eta_m - \eta_{-m}. \quad (15)$$

基于自参考对准原理的SMASH对准系统是目前先进对准系统的代表^[18],该对准系统通过对对准信号的解算得到对准标记的位置信息^[19]。本研究基于SMASH对准系统,从晶圆质量、信噪比和对准误差的角度,利用所提方法建立对准标记仿真模型分析对准

标记槽深、槽宽、膜层厚度和侧壁变形等参数对标记鲁棒性的影响,结合鲁棒性仿真结果给出对准系统提升工艺适应性的策略。

仿真用的入射场信息如表1所列,共有4个测量波长,每个波长有着确定的偏振态。对准标记采用业界使用较为广泛的AH53标记^[11],其正视图如图2所示。

表1 入射光波长和偏振态

Table 1 Wavelength and polarization state of incident light

| Incident wavelength /nm | Polarization state |
|-------------------------|--------------------|
| 532 | TE |
| 633 | TM |
| 780 | TE |
| 852 | TM |

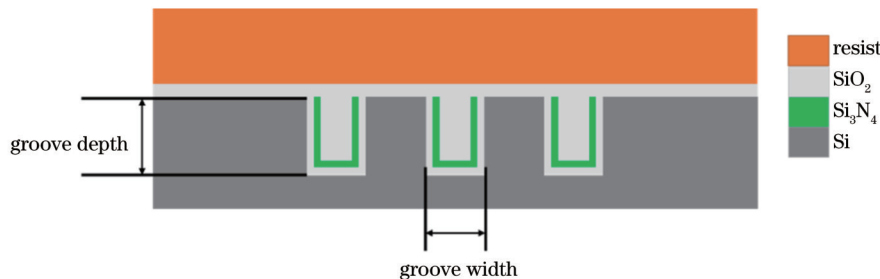


图2 AH53标记正视图

Fig. 2 Front view of AH53 mark

3.1 最佳空间谐波数的确定

空间谐波数是影响标记仿真精度和所需时间的关键因素,由文献[7]中空间谐波数的确定方法可知,某一偏振态下最佳空间谐波数由系统的最小入射波长、最大光栅周期和最深槽深等3个参数确定。且圆偏振态计算结果收敛时,TE偏振和TM偏振态的计算均会收敛。因此设置入射光为532 nm波长的圆偏振光,槽深为400 nm,计算测量级次(5级)衍射效率随空间谐波数的收敛情况,具体如图3所示,最终确定合适的空间谐波数为271。相对于文献[7]中没有工艺叠层和结构简单的对准标记,本研究的对准标记计算所需的空间谐波数明显增大。

3.2 槽深的鲁棒性分析及工艺适应性策略

利用光刻机生产不同器件时,对准标记的槽深会根据工艺需求而变化。结合工艺实际情况,研究槽深变化范围在[100 nm, 400 nm],利用所提方法构建了模型,以图2所示对准标记为例获得晶圆质量和信噪比随槽深变化的曲线,具体如图4所示。从图4可以看出,槽深变化会同时引起晶圆质量和信噪比发生近似周期性的变化,周期与测量光波长呈正相关。晶圆质量和信噪比随槽深变化会出现峰谷,且不同波长下峰谷的位置不同。为此,从光刻机设备研发的角度,可通过增加对准系统测量波长的个数,选择晶圆质量和信

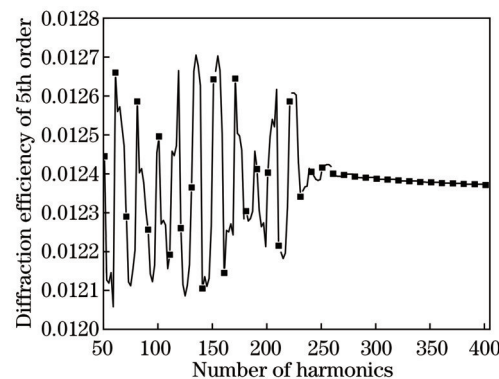


图3 不同谐波数下的5级衍射效率

Fig. 3 5th order diffraction efficiency at different harmonic numbers

噪比较高的信号通道作为测量信号可有效解决槽深变化对晶圆质量和信噪比的影响,从而提高对准系统的工艺适应性。

3.3 槽宽的鲁棒性分析及工艺适应性策略

槽宽在光刻工艺的影响下会偏离设计值。利用所建模型取图2所示对准标记的槽宽为1.6 μm,变化范围为±0.8 μm,仿真获得晶圆质量和信噪比随槽宽变化的曲线,如图5所示。可以看出,槽宽变化会同时引起晶圆质量和信噪比的变化,且晶圆质量和信噪比在波峰处变化比较平缓。相较于信噪比,晶圆质量受槽

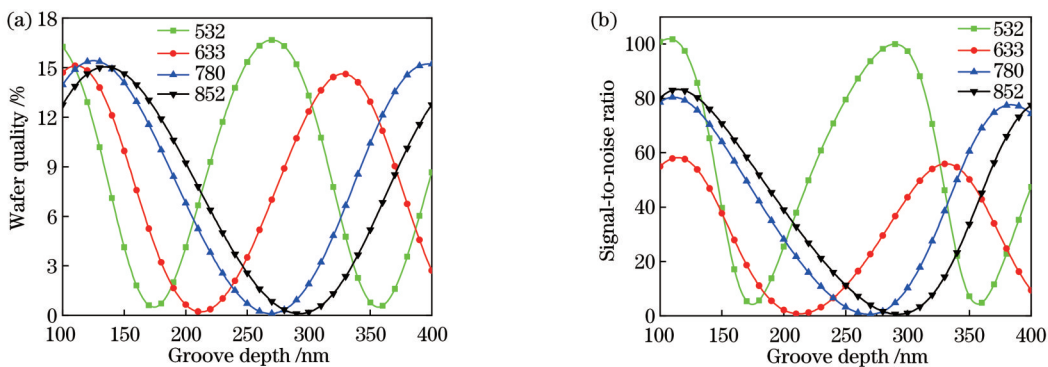


图4 晶圆质量和信噪比随槽深变化的曲线。(a)晶圆质量;(b)信噪比

Fig. 4 Curves of wafer quality and signal-to-noise ratio changing with groove depth. (a) Wafer quality;(b) signal-to-noise ratio

宽的影响更大。光刻机通过严格控制投影物镜波像差等因素,可使曝光图样的线宽控制在目标值±10%之

内^[20-21],在此范围内,对准标记的晶圆质量和信噪比变化幅度较小。

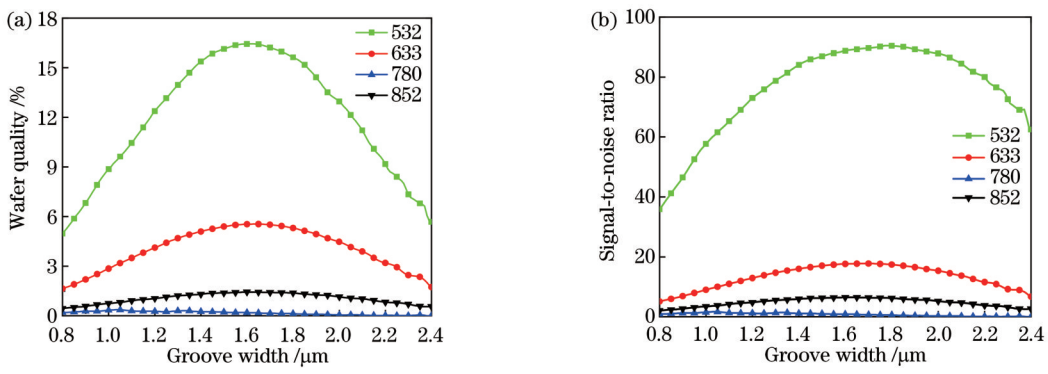


图5 晶圆质量和信噪比随槽宽变化的曲线。(a)晶圆质量;(b)信噪比

Fig. 5 Curves of wafer quality and signal-to-noise ratio changing with groove width. (a) Wafer quality;(b) signal-to-noise ratio

3.4 膜层厚度的鲁棒性分析及工艺适应性策略

对于不同的入射波长,膜层材料的折射率和吸收系数是不同的,膜层厚度的变化会直接导致测量信号强度和信噪比的变化。利用所建模型改变图2所示对准标记上覆盖的膜层厚度并进行仿真分析。当标记上覆盖光刻胶的厚度变化范围为±150 nm时,仿真获得晶圆质量和信噪比随光刻胶厚度变化的曲线,如图6所示。同理,当氧化层厚度在[0 nm, 300 nm]变化时,晶圆质量和信噪比的变化曲线如图7所示。从图6和

图7可知,晶圆质量和信噪比随膜层厚度变化的规律与随槽深变化的规律相似,但相较于晶圆质量,膜层厚度变化主要引起对准标记信噪比的变化。在实际生产过程中,受工艺的影响,光刻胶或氧化层厚度很难控制为某一固定值。结合仿真结果可知,不同波长的变化曲线不同,选择信噪比高的信号通道作为测量信号可有效解决膜层厚度变化对信噪比的影响,从而提高系统的工艺适应性。

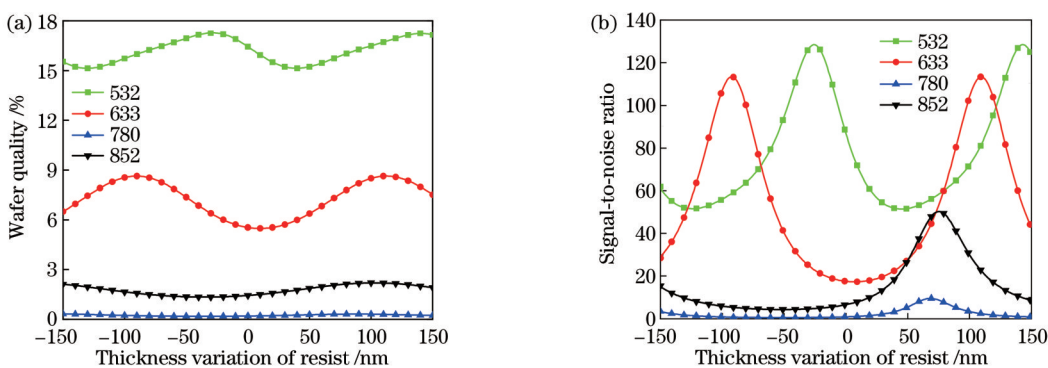


图6 晶圆质量和信噪比随光刻胶变化的曲线。(a)晶圆质量;(b)信噪比

Fig. 6 Curves of wafer quality and signal-to-noise ratio changing with resist. (a) Wafer quality;(b) signal-to-noise ratio

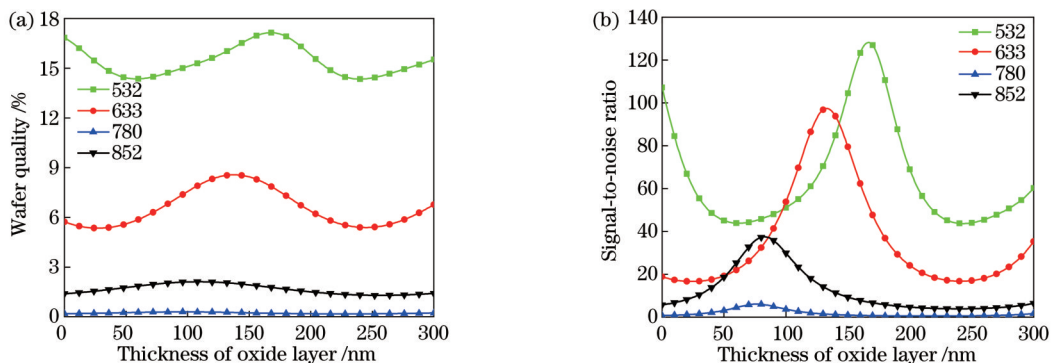


图7 晶圆质量和信噪比随氧化层变化的曲线。(a)晶圆质量;(b)信噪比

Fig. 7 Curves of wafer quality and signal-to-noise ratio changing with oxide layer. (a) Wafer quality; (b) signal-to-noise ratio

3.5 侧壁变形的鲁棒性分析及工艺适应性策略

3.5.1 最佳分层数目和空间谐波数的确定

受工艺影响,实际对准标记的侧壁会存在两种形

式的变形:一种是标记侧壁与槽底存在倾角,称为侧壁倾角变形;另一种是标记侧壁与槽底存在圆弧状变形,称为侧壁圆弧变形。两种变形如图8所示。

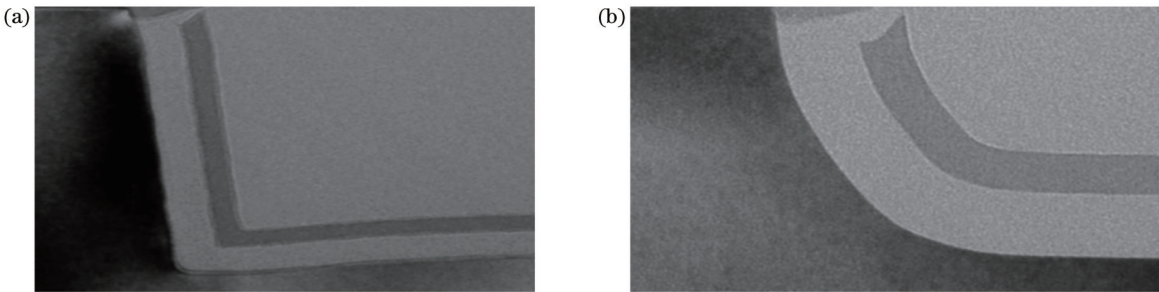


图8 侧壁变形示意图。(a)侧壁倾角变形;(b)侧壁圆弧变形

Fig. 8 Schematic diagrams of sidewall deformation. (a) Sidewall angle;(b) sidewall of arc

当对准标记存在侧壁变形时,需要使用严格耦合波法和分层近似法联合的方法进行仿真。由第2节可知,分层近似法中分层数目和严格耦合波法中空间谐波数均会对计算精度产生影响。基于SMASH系统,针对图2所示标记,研究不同波长、不同侧壁倾角下分层数目对计算精度的影响,具体如图9所示。由图9可知,随着分层数目的增大,计算结果收敛。入射波长和侧壁变形程度与最佳分层数目无明显关系。

结合文献[7]中空间谐波数的确定方法,研究了532 nm入射波长、圆偏振态、不同侧壁倾角下空间谐波数对计算精度的影响规律,结果如图10所示。可以看出,不同侧壁倾角下,空间谐波数对5级衍射效率的影响趋势十分相似,最佳谐波数基本相同,即最佳空间谐波数不受侧壁变形程度的影响。

综合以上仿真结果,取最佳分层数为200,最佳谐波数为271。

3.5.2 对称侧壁倾角的鲁棒性分析及工艺适应性策略

根据确定的最佳分层数目和空间谐波数,利用所建模型仿真获得晶圆质量和信噪比随侧壁倾角变化的曲线,如图11所示。由图11可知,侧壁倾角变化对晶

圆质量和信噪比的总体影响不大。

3.5.3 对称圆弧侧壁的鲁棒性分析及工艺适应性策略

因工艺不同,对准标记的侧壁变形呈圆弧形状,圆弧形变方向有两种:凸圆弧侧壁和凹圆弧侧壁,如图12所示^[19]。

生产工艺不同,圆弧变形程度不同。利用所建模型对图12(a)所示的3种不同程度的凹圆弧侧壁情况进行仿真,结果如图13所示。对图12(b)所示的3种不同程度的凸圆弧侧壁情况进行仿真,结果如图14所示。由图13和14可知,凹圆弧侧壁与凸圆弧侧壁变化对晶圆质量和信噪比的影响不大。

综上所述,考虑到实际加工水平,侧壁变形程度不会超出本研究仿真范围。从对准的角度分析,即其鲁棒性较好,不需要采取针对性的工艺适应性策略。

3.5.4 非对称侧壁的鲁棒性分析及工艺适应性策略

当对准标记发生左右侧壁倾角不同的变形时(如左侧侧壁倾角为100°,右侧侧壁倾角为110°),且内部材料也发生相应变形,标记变形示意图如图15所示。

基于仿真模型对变形标记进行仿真,测量级次(5级)衍射效率仿真结果如表2所示。由仿真结果可知,正负级次测量信号的衍射效率存在差异,即非对称变

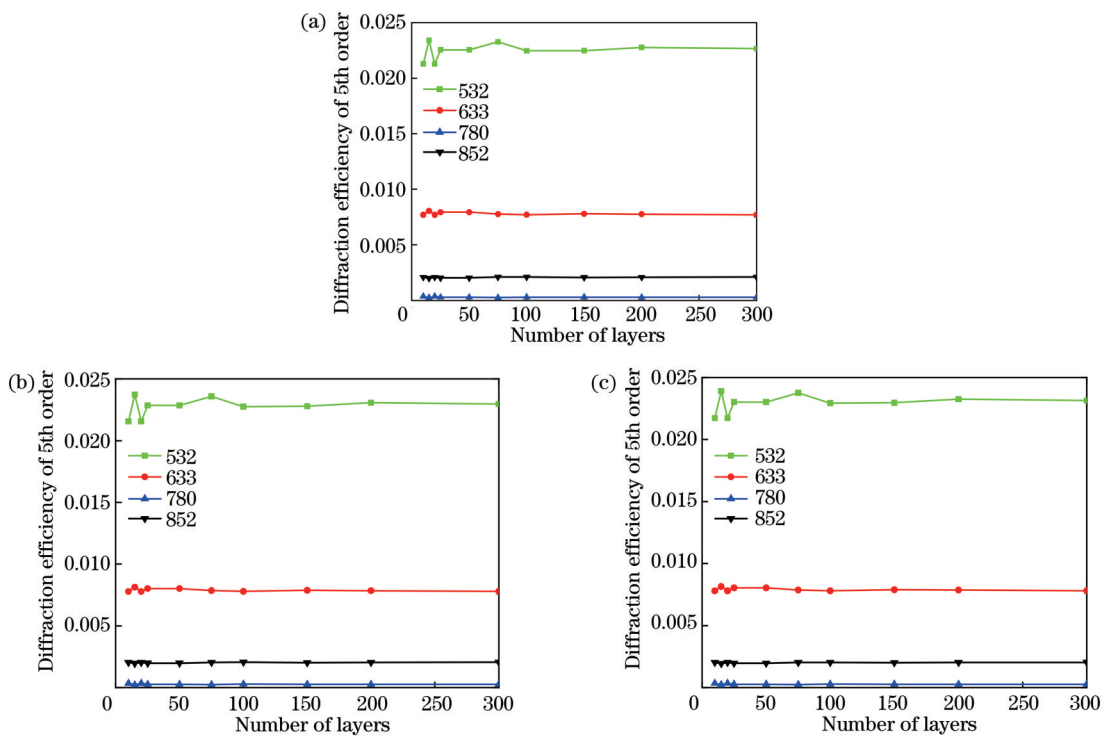


图9 不同侧壁倾角分层数目对计算精度的影响。(a) 120°;(b) 110°;(c) 100°

Fig. 9 The influence of the number of layers on the calculation accuracy under different sidewall angles. (a) 120°; (b) 110°; (c) 100°

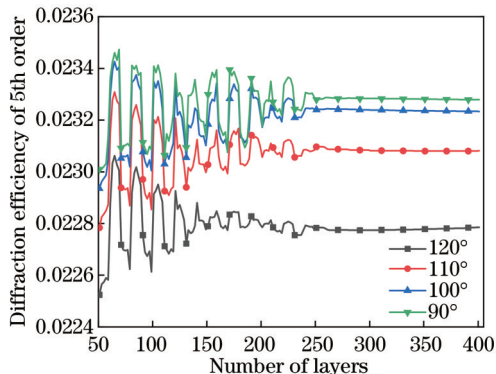


图10 不同侧壁倾角下空间谐波数对计算精度的影响

Fig. 10 The influence of number of harmonic on calculation accuracy under different sidewall angles

形会使对准系统产生对准误差。为此,一方面通过工艺优化尽量减小非对称变形,另一方面在非对称变形不可避免时,利用对准位置偏移量与入射波长相关这一特征,通过解算多个波长下的权重最终获得存在变形时的正确对准位置^[22],从而提升系统的工艺适应性。

4 仿真和实验验证

为验证所建模型的正确性,结合文中公式与相同原理的VirtualLab商业软件对图2所示的对准标记进行仿真,结果如图16所示。可以看出,仿真结果与所提模型仿真结果相同,验证了所建模型的正确性。

为进一步证明所提方法的有效性和准确性,借助光刻机制备了对准标记,并测量了标记的晶圆质量,如图17所示。将对准标记切片,并利用电子显微镜测量,该标记为存在侧壁倾角的变形标记,如图18所示。切片测量参数输入仿真模型,仿真结果与实验结果如图19所示。由图19可知,仿真结果与实验测量结果基本相同,验证了所提方法的有效性和准确性。仿真结果和实验结果之间的轻微差异,推测是光刻机测量基准标记衍射效率与仿真输入值略有差异导致的。

5 结 论

针对复杂结构对准标记的仿真需求,联合严格耦合波法和分层近似法提出一种对准标记鲁棒性分析方

表2 非对称标记仿真结果
Table 2 Simulation results of asymmetric mark

| Incident wavelength /nm | Diffraction efficiency of -5th /% | Diffraction efficiency of 5th /% |
|-------------------------|-----------------------------------|----------------------------------|
| 532 | 2.21 | 2.19 |
| 633 | 0.72 | 0.76 |
| 780 | 0.04 | 0.03 |
| 852 | 0.20 | 0.18 |

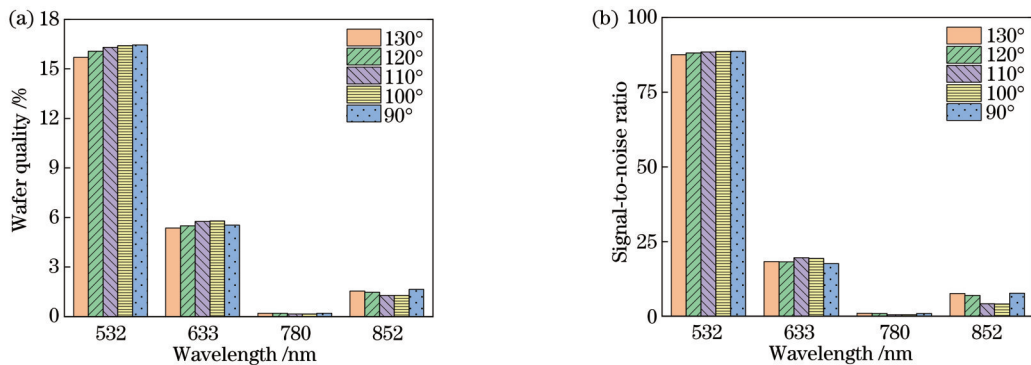


图11 晶圆质量和信噪比随侧壁倾角变化的曲线。(a)晶圆质量;(b)信噪比

Fig. 11 Curves of wafer quality and signal-to-noise ratio changing with sidewall angle. (a) Wafer quality; (b) signal-to-noise ratio

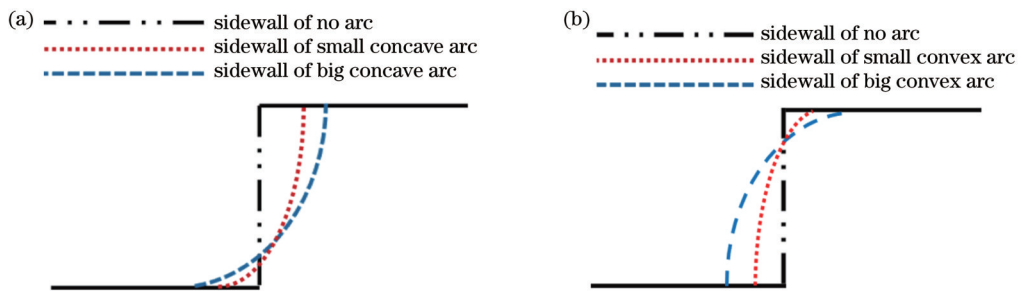


图12 圆弧侧壁示意图。(a)凹圆弧侧壁;(b)凸圆弧侧壁

Fig. 12 Schematic diagrams of sidewall of arc. (a) Sidewall of concave arc; (b) sidewall of convex arc

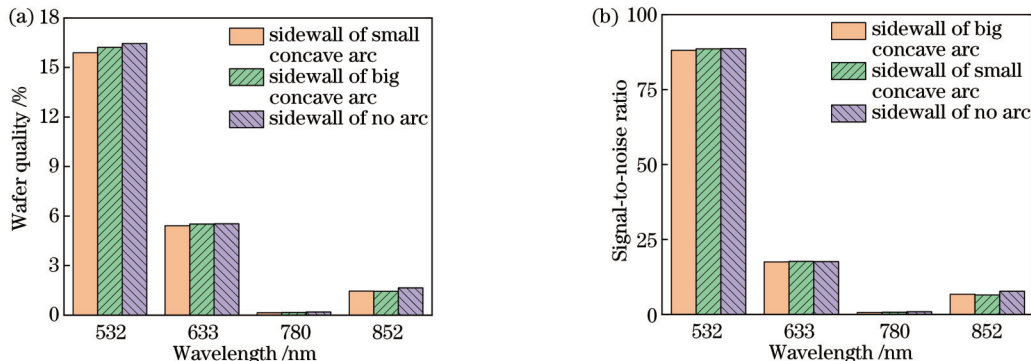


图13 晶圆质量和信噪比随凹圆弧侧壁变化的曲线。(a)晶圆质量;(b)信噪比

Fig. 13 Curves of wafer quality and signal-to-noise ratio changing with sidewall of concave arc. (a) Wafer quality; (b) signal-to-noise ratio

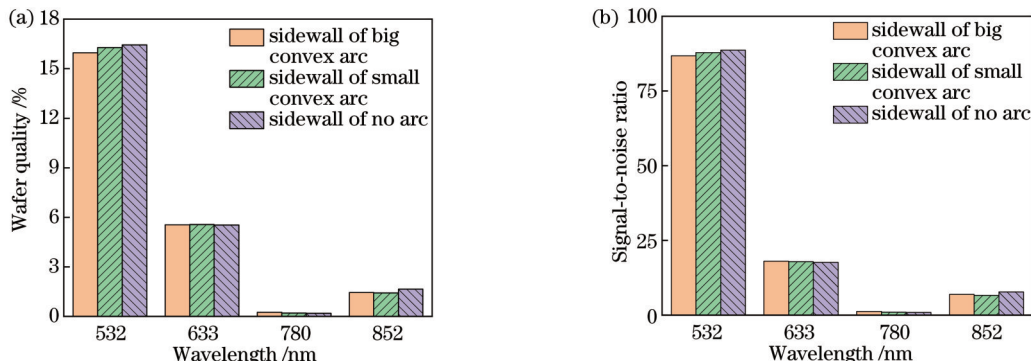


图14 晶圆质量和信噪比随凸圆弧侧壁变化的曲线。(a)晶圆质量;(b)信噪比

Fig. 14 Curves of wafer quality and signal-to-noise ratio changing with sidewall of convex arc. (a) Wafer quality; (b) signal-to-noise ratio

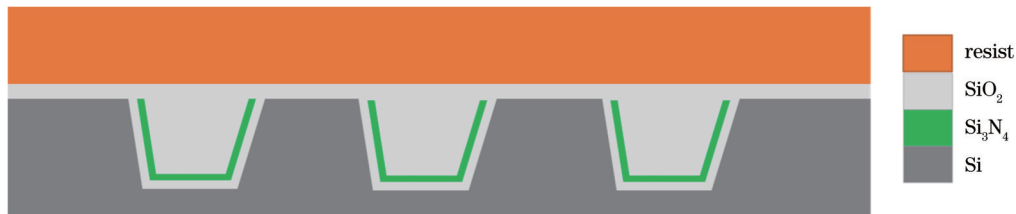


图15 非对称标记示意图
Fig. 15 Schematic diagram of asymmetric mark

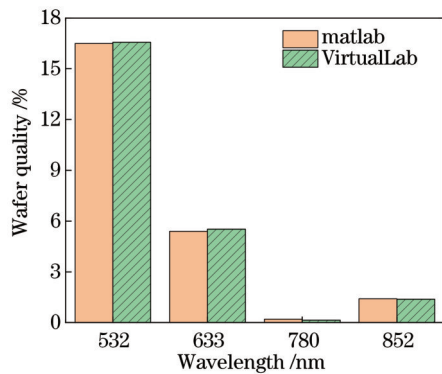


图16 两种方法的仿真结果对比
Fig. 16 Comparison of simulation results of two methods

法，并构建了仿真模型。以晶圆质量和信噪比为评价函数，研究了槽深、槽宽、膜层厚度和侧壁对称变形等参数对标记鲁棒性的影响；以对准误差为评价函数，研究了侧壁非对称变形对标记鲁棒性的影响。并结合对准标记鲁棒性分析结果明晰了光刻机提升标记工艺适应性的策略。最后借助VirtualLab商业软件验证了所

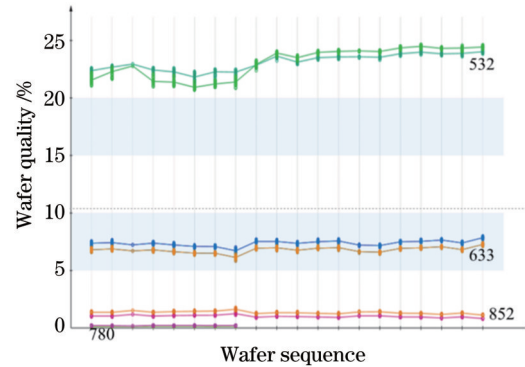


图17 标记的晶圆质量测量
Fig. 17 Marked wafer quality measurement

建模型的正确性，并在光刻机上制作标记进行了实验测试，仿真结果和实验结果一致，验证了所提方法的有效性和准确性。所提方法和给出的工艺适应性策略，对于对准标记设计优化和光刻机对准精度提升具有重要的理论意义和应用价值。

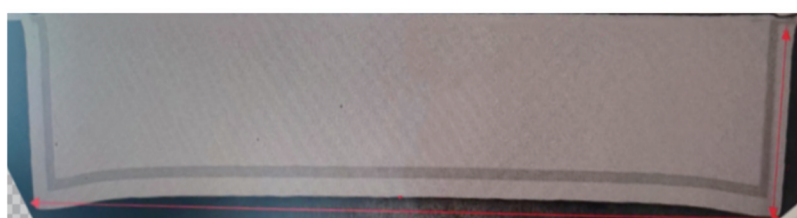


图18 标记横截面
Fig. 18 Cross section of mark

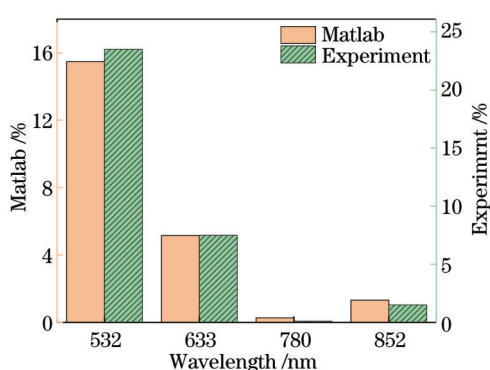


图19 仿真结果与实验结果对比
Fig. 19 Comparison between simulation results and experimental results

参 考 文 献

- [1] Chen X W, Chen L, Wang Y, et al. AgGeSbTe thin film as a negative heat-mode resist for dry lithography[J]. Chinese Optics Letters, 2022, 20(3): 031601.
- [2] Wang S M, Zhao J H, Gu J J, et al. LiNbO₃ channel and ridge waveguides based on helium ion implantation combined with lithography and precise diamond dicing[J]. Chinese Optics Letters, 2022, 20(7): 071301.
- [3] 杜聚有, 戴凤钊, 王向朝. 标记非对称变形导致的对准误差修正方法及其在套刻测量中的应用[J]. 中国激光, 2019, 46(7): 0704004.
Du J Y, Dai F Z, Wang X Z. Calibration method for alignment error caused by asymmetric deformation of mark and its application in overlay measurement[J]. Chinese Journal of Lasers, 2019, 46(7): 0704004.

- [4] 杨光华, 王宇, 李璟, 等. 相位光栅非对称性对位置测量精度的影响[J]. 光学学报, 2021, 41(19): 1905001.
Yang G H, Wang Y, Li J, et al. Effect of phase grating asymmetry on position measurement accuracy[J]. Acta Optica Sinica, 2021, 41(19): 1905001.
- [5] Cui Y T, Goodwin F, van Haren R. Segmented alignment mark optimization and signal strength enhancement for deep trench process[J]. Proceedings of SPIE, 2004, 5375: 1265-1277.
- [6] 杜聚有. 基于位相衍射光栅的投影光刻机对准技术研究[D]. 北京: 中国科学院大学, 2019: 80-87.
Du J Y. Research on projection mask aligner alignment technology based on phase diffraction grating[D]. Beijing: University of Chinese Academy of Sciences, 2019: 80-87.
- [7] 周光迎, 齐月静, 齐威, 等. 共振域相位光栅标记设计方法[J]. 光学学报, 2022, 42(21): 2105001.
Zhou G Y, Qi Y J, Qi W, et al. Design method of phase grating mark in resonance domain[J]. Acta Optica Sinica, 2022, 42(21): 2105001.
- [8] 杨光华, 王宇, 李璟, 等. 增强型相位光栅衍射效率研究[J]. 光学学报, 2021, 41(12): 1205001.
Yang G H, Wang Y, Li J, et al. Diffraction efficiency of enhanced phase grating[J]. Acta Optica Sinica, 2021, 41(12): 1205001.
- [9] Li L, Chen C, Zeng H, et al. Analysis of diffraction-based wafer alignment rejection for thick aluminum process[J]. Journal of Vacuum Science and Technology, 2022, 40(2): 022603.
- [10] Wu Q, Williams G, Kim B Y, et al. Ultrafast wafer alignment simulation based on thin film theory[J]. Proceedings of SPIE, 2002, 4689: 364-373.
- [11] Zhang L, Dong L, Su X, et al. New alignment mark designs in single patterning and self-aligned double patterning[J]. Microelectronic Engineering, 2017, 179: 18-24.
- [12] Shin J, Chalykh R, Kang H, et al. Overlay metrology for dark hard mask process: simulation and experiment study[J]. Proceedings of SPIE, 2007, 6518: 65182U.
- [13] Yun S, Ha S M, Nam Y M, et al. A comparison of alignment and overlay performance with varying hardmask materials[J]. Proceedings of SPIE, 2012, 8324: 832407.
- [14] Ahn J K, Ha J H, Kim H I, et al. Optimization of alignment strategy for metal layer on local interconnect integration[J]. Proceedings of SPIE, 2009, 7272: 7272-1-7272-10.[LinkOut]
- [15] 陈琪, 李国俊, 方亮, 等. 亚波长多台阶结构大角度激光分束器设计[J]. 中国激光, 2016, 43(2): 0205006.
Chen Q, Li G J, Fang L, et al. Design of wide-angle laser beam splitter with sub-wavelength multi-level structure[J]. Chinese Journal of Lasers, 2016, 43(2): 0205006.
- [16] 赵华君. 亚波长光栅光学[M]. 成都: 西南交通大学出版社, 2017.
Zhao H J. Subwavelength grating optics[M]. Chengdu: Southwest Jiaotong University Press, 2017.
- [17] 郝义伟, 孔新新, 才啟胜, 等. 环形器噪声对激光干涉测量系统影响分析[J]. 光学学报, 2021, 41(9): 0912003.
Hao Y W, Kong X X, Cai Q S, et al. Analysis of effect of circulator noise on laser interferometry system[J]. Acta Optica Sinica, 2021, 41(9): 0912003.
- [18] Leray P, Jehoul C, Socha R, et al. Improving scanner wafer alignment performance by target optimization[J]. Proceedings of SPIE, 2016, 9778: 9778M.
- [19] 徐孟南, 卢增雄, 齐月静, 等. 光束偏振对自参考干涉信号对比度的影响[J]. 激光与光电子学进展, 2021, 58(23): 2326002.
Xu M N, Lu Z X, Qi Y J, et al. Influence of beam polarization on contrast of self-referencing interference signal[J]. Laser & Optoelectronics Progress, 2021, 58(23): 2326002.
- [20] 韦亚一. 超大规模集成电路先进光刻理论与应用[M]. 北京: 科学出版社, 2016.
Wei Y Y. Theory and application of advanced lithography for VLSI[M]. Beijing: Science Press, 2016.
- [21] Hermans J V, Baudemprez B, Lorusso G, et al. Stability and imaging of the ASML EUV alpha demo tool[J]. Proceedings of SPIE, 2009, 7271: 72710T.
- [22] Jeong I H, Kim H S, Kong Y O, et al. Improved wafer alignment model algorithm for better on-product overlay[J]. Proceedings of SPIE, 2019, 10961: 10961-1-10961.

Robustness Analysis Method and Simulation Research of Alignment Mark

Zhou Guangying^{1,3}, Qi Yuejing^{1,3*}, Li Liang², Jiang Miao², Shi Jiangliu², Yao Mingyi^{1,3}

¹Institute of Microelectronics of the Chinese Academy of Sciences, Beijing 100029, China;

²Beijing Superstring Academy of Memory Technology, Beijing 100176, China;

³University of Chinese Academy of Sciences, Beijing 100049, China

Abstract

Objective With the continuously shrinking lithography process nodes, new materials, and technologies are constantly introduced, which exerts different effects on the mark in the lithography machine alignment system. Therefore, improving the robustness of alignment marks is crucial for high-precision alignment. It takes extensive time and cost to verify the robustness of alignment marks based on experimental methods. The industry tends to adopt simulation experiments to improve research efficiency and economy. The theory of alignment mark simulation can be divided into scalar diffraction theory and vector diffraction theory. For alignment marks with small periods or complex structures, the rigorous coupled wave method in vector diffraction theory has good computational accuracy and speed. For the alignment mark simulation with complex structures, a robustness analysis method of alignment marks is proposed by combining the rigorous coupled wave method and the layered approximation method. The robustness of marks is analyzed by this method, and the lithography strategy of improving the process adaptability of the mark is clarified with the analysis results. The proposed method and the given process adaptability strategy show theoretical significance and application value for the alignment

mark design and alignment accuracy of scanners.

Methods For the ideal mark with the standard surface, a vector diffraction simulation model can be built by the rigorous coupled wave method. For alignment marks with sidewall deformation due to process influence, it is difficult to directly establish the surface function, as the surface is non-standard anymore. Therefore, a robust analysis method of alignment marks is proposed by combining the rigorous coupled wave method and the layered approximation method to meet the requirements. The alignment mark with sidewall deformation is divided into multiple layers with equal thickness. When the number of layers is large enough, each layer can be approximated as a rectangular structure. The alignment mark with complex structure can be replaced by a whole composed of multiple rectangular structures. The rectangular structure in each layer is analyzed according to the rectangular grating method. Then the Maxwell equations and boundary conditions of each layer and region are combined. Finally, the diffraction efficiency of the alignment mark with complex structure is calculated. Wafer quality (WQ), signal-to-noise ratio (SNR), and alignment error are three important factors affecting measurement accuracy, which are employed as evaluation functions to study the robustness of alignment marks.

Results and Discussions With WQ and SNR as the evaluation functions, the effects of the changes in groove depth, groove width, film thickness, and sidewall symmetry deformation on mark robustness are studied. The changes in groove depth, groove width, and film thickness cause the WQ and SNR to change approximately and periodically. The period is positively correlated with the measured optical wavelength. Under different wavelengths, the WQ and SNR show different peaks and valleys along with these parameter changes (Figs. 4–7). Therefore, the problem that these changes affect WQ and SNR can be solved by increasing the number of measurement wavelengths of the alignment system and selecting the signal channel with WQ and SNR as the measurement signal to improve the process adaptability of the alignment system. Symmetrical sidewall deformation shows little impact on the WQ and SNR of the mark, making it unnecessary to take targeted process adaptation strategies (Figs. 11–14). With the alignment error as the evaluation function, the robustness of the sidewall asymmetric deformation mark is studied. The diffraction efficiency of positive and negative order measurement signals of this mark is different, indicating that the alignment error is introduced (Table 2). With an aim to reduce the alignment error, on one hand, the asymmetric deformation is minimized through process optimization. On the other hand, the correct alignment position in the presence of deformation is obtained by solving the weights under multiple wavelengths. Finally, the correctness of the model is verified by the VirtualLab commercial software, and the marks are set up on the scanner for experimental testing. The simulation results are consistent with the experimental results, thus verifying the effectiveness and accuracy of the proposed method.

Conclusions In this study, a robustness analysis method of alignment marks is proposed by combining the rigorous coupled wave method and the layered approximation method based on the simulation requirements of alignment marks for complex structures. The simulation model is built by this method. This paper analyzes the effects of groove depth, groove width, film thickness, and sidewall deformation on mark robustness. The changes in groove depth, groove width, and film thickness cause the WQ and SNR to change approximately and periodically. Additionally, the period is positively correlated with the measured optical wavelength. Under different wavelengths, the WQ and SNR show different peaks and valleys along with these parameter changes. Symmetrical sidewall deformation shows little impact on the WQ and SNR of the mark, whereas the mark deformation of asymmetric deformation introduces alignment error. The lithography strategy of improving the process adaptability of the mark is clarified with the analysis results. With the assistance of VirtualLab commercial software and the experimental platform, the validity and accuracy of the analysis method are verified. The research results in this paper show theoretical significance and application value for the alignment mark design and the alignment accuracy of scanners.

Key words lithography; alignment mark; rigorous coupled wave method; layered approximation method; robustness; process adaptability